

The role of clearance mechanisms in the kinetics of toxic protein aggregates involved in neurodegenerative diseases.

Travis B. Thompson*, Georg Meisl†, Tuomas Knowles†‡, and Alain Goriely*

*Mathematical Institute, Andrew Wiles Building
Woodstock Rd University of Oxford OX2 6GG, UK

†Centre for Misfolding Diseases, Department of Chemistry,
University of Cambridge, Lensfield Road, Cambridge CB2 1EW, UK

‡Cavendish Laboratory, University of Cambridge,
19 JJ Thomson Avenue, Cambridge CB3 0HE, UK

September 30, 2020

Abstract

Protein aggregates in the brain play a central role in cognitive decline and structural damage associated with neurodegenerative diseases. For instance, in Alzheimer’s disease the formation of Amyloid-beta plaques and tau proteins neurofibrillary tangles follows from the accumulation of different proteins into large aggregates through specific mechanisms such as nucleation and elongation. These mechanisms have been studied in vitro where total protein mass is conserved. However, in vivo, clearance mechanisms may play an important role in limiting the formation of aggregates. Here, we generalize classical models of protein aggregation to take into account both production of monomers and the clearance of protein aggregates. Depending on the clearance model, we show that there may be a critical clearance value above which aggregation does not take place. Our result offers further evidence in support of the hypotheses that clearance mechanisms play a potentially crucial role in neurodegenerative disease initiation and progression; and as such, are a possible therapeutic target.

1 Introduction

Alzheimer’s disease (AD), and other related neurodegenerative diseases, are associated with the assembly of specific, toxic proteins into fibrillar aggregates. Alzheimer’s disease, in particular, is characterized by the aggregation of Amyloid- β ($A\beta$) plaques and tau protein neurofibrillary tangles (NFT). The role of $A\beta$ in Alzheimer’s is thought to be so central to the disease that it is the basis of the so-called ‘Amyloid- β hypothesis’ [1, 2, 3], stating that the accumulation and deposition of oligomeric or fibrillar amyloid beta peptide is the main cause of the disease. This hypothesis has provided a guide for most of AD research over the last 20 years. However, recent experimental

evidence, and the failure of several drug trials, has led to renewed scrutiny of this foundational assumption.

The production of $A\beta$ is a natural process related to neuronal activity. Indeed, $A\beta$ is a normal metabolic waste byproduct [4, 5] that is typically removed from intracellular and extracellular compartments by several clearance mechanisms [6, 7]. In healthy subjects waste proteins are broken down by enzymes, removed by cellular uptake, or efflux to cerebrospinal fluid compartments where they eventually reach arachnoid granulations, or lymphatic vessels. While healthy clearance mechanisms, working in harmony, avert the buildup of toxic $A\beta$ plaques and tau NFT; their impairment or dysfunction can lead to toxic levels of aggregates [7]. The specifics of in-vivo clearance mechanisms remain a topic of clinical debate; however, the kinetics enabling proteins to amass into toxic aggregates can be carefully, and systematically, studied in vitro and under varied conditions. The production of $A\beta$, at a high level, is mediated by a membrane protein called amyloid precursor protein (APP). APP is typically cleaved by α -secretase and the resulting products do not aggregate. However, APP can also be cleaved by β -secretase, which results in soluble monomeric APP fragments of different sizes. The most common size categories are $A\beta_{38}$, $A\beta_{40}$, and $A\beta_{42}$. While monomeric $A\beta_{38}$ is not prone to further aggregation; $A\beta_{40}$ and $A\beta_{42}$, containing two additional amino acids at the C terminus, are the main isoforms of interest in the study of AD pathology.

Protein aggregation pathways are, in general, complex and involve multiple steps. In fact, it has recently been shown [8] that the aggregation properties of $A\beta_{40}$, which is more abundant, differ from those of the more aggregate-prone $A\beta_{42}$; even under the same conditions. A theoretical framework of chemical kinetics and aggregation theory [9, 10, 11] has been combined with careful, systematic in vitro experiments performed under differing conditions; such as varied concentration or pH. This approach has: elucidated effective pathways and mechanisms for nucleation, aggregation and fragmentation [12]; and produced a deep understanding of key properties, underlying the formation of aggregates under ideal conditions, with the potential for therapeutic intervention [13, 14].

Here, we develop a mathematical framework to describe the effects of clearance and monomer production chemical kinetics driving aggregation; we apply the framework to the study of $A\beta$. To accomplish this, we extend the current theory describing $A\beta$ aggregation in vitro, which has been validated against experiment, to include monomer production and oligomer clearance terms. In particular, we study two different clearance mechanisms: one where total mass is conserved (size-independent clearance); and one where it is not (size-dependent clearance). In the former case we show the full system reduces to three equations amenable to a systematic analysis. We identify a critical value of clearance above which the production of toxic aggregates does not take place. Our results offer further evidence in support of two main hypotheses: that clearance mechanisms play a crucial role in neurodegenerative disease initiation and progression; and that therapies enhancing clearance above a prescribed, critical value may serve as a possible intervention strategy. In particular, we will exhibit the existence of critical clearance values; such values are consistent with the observation of disease onset when natural clearance mechanisms within the brain have degraded through aging.

2 A model of toxic protein aggregation

Our model for protein aggregation-dynamics model includes multiple mechanisms: heterogeneous primary nucleation; homogeneous primary nucleation; secondary nucleation; linear elongation; frag-

mentation; and clearance (c.f. Fig. 1). These mechanisms lead to a general class of mathematical models that can describe a wide range of aggregating systems in vitro. In particular, by including heterogeneous primary nucleation terms, a source term for new nuclei, that is independent of monomer concentration, is present; this source is in addition to the usual monomer-dependent homogeneous primary nucleation. Thus, in such a model, the importance of interfaces in the initiation of nucleation is sufficiently accounted for. In the model, each aggregate of a given size is represented by a population. In general, each population, with aggregates of size i , will be represented by an indexed concentration; we use the special notation $m(t)$ for the monomer population $i = 1$, while all other aggregate concentrations are denoted by $p_i(t)$ for $i \in \{2, 3, \dots\}$. The master equations are then:

$$\frac{dm}{dt} = \gamma - \lambda_1 m - 2k_0 - n_c k_n m^{n_c} - 2k_+ m P - n_2 k_2 \sigma(m) M + 2k_{\text{off}} P \quad (1)$$

$$\frac{dp_2}{dt} = -\lambda_2 p_2 + k_0 + \delta_{2,n_c} k_n m^{n_c} - 2k_+ m p_2 + \delta_{2,n_2} k_2 \sigma(m) M + 2k_{\text{off}} p_3 \quad (2)$$

$$\frac{dp_i}{dt} = -\lambda_i p_i + \delta_{i,n_c} k_n m^{n_c} + 2k_+ m (p_{i-1} - p_i) + 2k_{\text{off}} (p_{i+1} - p_i) + \delta_{i,n_2} k_2 \sigma(m) M, \quad i > 2, \quad (3)$$

where $\delta_{i,j}$ is Kronecker's delta (1 if $i = j$ and 0 otherwise) and

$$\sigma(m) = \frac{m^{n_2} K_M}{K_M + m^{n_2}}, \quad P = \sum_{i=2}^{\infty} p_i, \quad M = \sum_{i=2}^{\infty} i p_i. \quad (4)$$

Here, P and M are the first two moments of the population distribution; they represent the total number and total mass of aggregates, respectively. In these equations, the parameters represent the following effects, sketched in Fig. 1: γ : (constant) monomer production such as by β -secretase mitigated cleavage of APP, driving mass influx; λ_i : clearance of aggregate of size i such as by lymphatic or cellular processes; k_0 : heterogeneous primary nucleation (independent of the monomer concentration); k_n and n_c : nucleation of aggregates of size $n_c > 1$; k_+ : linear elongation transforming aggregate from size i to $i + 1$; k_2 : secondary nucleation of aggregates of size $n_2 > 1$; K_M : saturation of the secondary nucleation; k_{off} : depolymerization by one monomer.

The aggregation model (1)-(3), and its many variations, have served as a template for in vitro experiments [8, 13, 15]. Multiple experimental fittings have shown that the exponents n_c and n_2 are: $n_c = n_2 = 2$ for A β 40 and for A β 42 in the presence of a PBS buffer [8, 15]; for A β 42 in the presence of a HEPES buffer $n_2 = 2$ and $n_c = 0$ provides the best fit [13]. For the discussions and derivations in this manuscript we take the view of PBS buffer experiments [8, 15] so that $n_c = n_2 = 2$. Adaptation to A β 42 HEPES, so that $n_c = 0$, is straightforward and all numerical results are qualitatively similar. When fitting experimental data it is often the case that only one of k_0 or k_n , depending on the best data fit, is used; i.e. that either heterogeneous primary nucleation or homogeneous primary nucleation best explains the particular experimental data.

The primary purpose of this manuscript is to describe the qualitative impact of clearance mechanisms in the dynamics and a particular choice of nucleation mechanism, i.e. $k_0 = 0$ versus $k_n = 0$, does not affect the results. Examples of fitted A β model parameters are listed in Table 1. PBS and HEPES refer to the buffers used in the corresponding experiments. Aggregation, in the fitted experiments, proceeds much faster than depolymerization and $k_{\text{off}} = 0$ is found to be a good fit to describe the dynamics. However, from a theoretical point of view, we note that $k_{\text{off}} = 0$ implies that

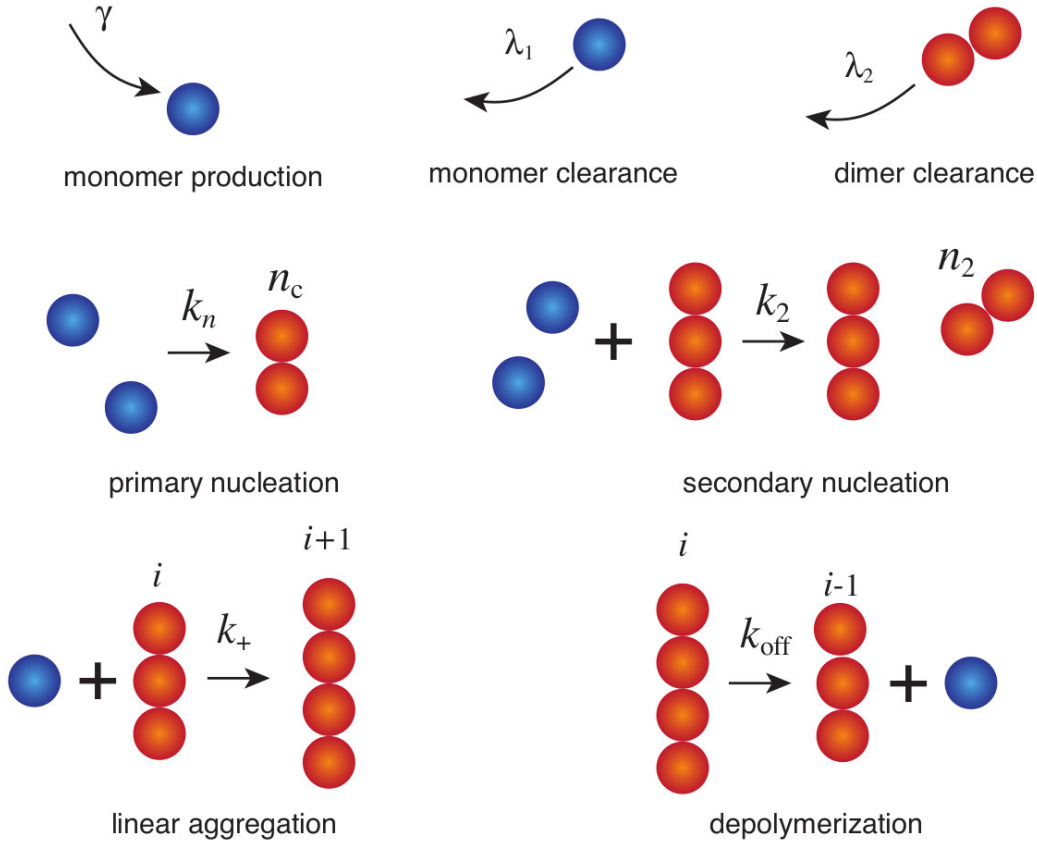


Figure 1: Mechanisms included in the master equations (1)-(3). We consider multiple effects for the formation of aggregates into our systems with rates constants k_i . The constants corresponding to transfer of mass to and from the external system are represented by greek letters (γ and λ_i). The process of heterogeneous nucleation (with constant k_0) is similar to homogeneous primary nucleation and is not depicted (the main difference being that its rate does not depend on the monomer concentration).

there is no non-vanishing stationary distribution in the absence of clearance and production terms. Here, we will first follow experimental data and take $k_{\text{off}} = 0$. Then, we will show that the addition of this small term does not change our results. Therefore, we will use the fitted experimental parameters given in Table 1. Clearance and production have not been investigated experimentally; thus, we leave them as free parameters. In particular, we will be interested in determining particular values of these parameters when a qualitative change of the dynamics occurs.

3 Size-independent clearance

In the case of size-independent clearance, we have $\lambda_i = \lambda > 0$ for all i . Our main question is to understand the role of the clearance term. In particular, we will establish that if clearance is sufficiently large, the formation of aggregates does not take place.

Table 1: Typical parameters for the $A\beta$ model. PBS and HEPES refer to the buffer used for the experiments. Note that A β 42 is generally faster than A β 40 and HEPES buffer is faster than PBS. In these experiments, aggregation is sufficiently fast so that $k_{\text{off}} = 0$ provides a good fit. The values of λ_{crit} give the critical values of clearance and their approximations for the size-independent case (see text). The values of τ_1 and τ_2 give the typical time scales associated with each dynamics (see text).

param.	mechanism	A β 40 PBS [15]	A β 42 PBS [8]	A β 42 HEPES [16]	units
k_0	heterogeneous nucleation	0	0	1.6×10^{-11}	M h^{-1}
k_n	homogeneous nucleation	5.8×10^{-3}	1.2×10^{-1}	0	$\text{M}^{1-n_c} \text{h}^{-1}$
n_c	homogeneous nucleation	2	2	2	unitless
k_2	secondary nucleation	1.1×10^7	3.6×10^7	2.1×10^{14}	$\text{M}^{-2} \text{h}^{-1}$
n_2	secondary nucleation	2	2	2	unitless
K_M	saturation	3.6×10^{-11}	3.6×10^{-12}	2.3×10^{-17}	M^2
k_+	elongation	1.1×10^9	1.1×10^{10}	1×10^{10}	$\text{M}^{-1} \text{h}^{-1}$
k_{off}	depolymerization	0	0	0	h^{-1}
m_0	Initial monomer c.	3×10^{-6}	3×10^{-6}	3×10^{-6}	M
λ_{crit}	critical clearance	0.72	2.45	17.0	h^{-1}
$\tilde{\lambda}_{\text{crit}}$	perfect bifurcation	0.72	2.47	17.0	h^{-1}
α	nonlinear coefficient	312,042	647,390	2.83726×10^6	$\text{M}^{-1} \text{h}^{-1}$
τ_1	exponential time scale	1.4	0.4	0.06	h
τ_2	amplification time scale	12.6	2.5	0.4	h
$\lambda_{\text{crit}}^{(1)}$	critical clearance $\nu = 1$	7.8×10^{-5}	9.2×10^{-5}	4.8×10^{-3}	h^{-1}
$\lambda_{\text{crit}}^{(0)}$	critical clearance $\nu = 0$	0.72	2.47	17.0	h^{-1}
$\lambda_{\text{crit}}^{(-1)}$	critical clearance $\nu = -1$	13.2×10^3	13.2×10^4	12×10^4	h^{-1}

3.1 Moment analysis

In the size-independent case, a well-known but remarkable feature of the system (1)-(3) is that a closed system of equations for the first two moments P and M and the monomer concentration $m = p_1$ can be obtained exactly:

$$\frac{dP}{dt} = -\lambda P + k_0 + k_n m^2 + k_2 \sigma(m) M, \quad (5)$$

$$\frac{dM}{dt} = -\lambda M + 2k_0 + 2(k_+ m - k_{\text{off}}) P + 2k_n m^2 + 2k_2 \sigma(m) M, \quad (6)$$

$$\frac{dm}{dt} = \gamma - \lambda m - 2k_0 - 2(k_+ m - k_{\text{off}}) P - 2k_n m^2 - 2k_2 \sigma(m) M, \quad (7)$$

where $\sigma(m) = m^2 K_M / (K_M + m^2)$ and we have chosen $n_2 = 2$. The total mass of the system $M_{\text{tot}} = M + m$ satisfies, by summing (6)-(7), the evolution equation

$$\frac{dM_{\text{tot}}}{dt} = -\lambda M_{\text{tot}} + \gamma. \quad (8)$$

This equation implies that the total mass in the system evolves to a stable steady state $M_{\text{tot}} = \gamma/\lambda$ with a typical time-scale $1/\lambda$. To simplify the analysis, we will further assume that, initially, the

system is at this state by choosing the following unseeded initial conditions

$$M(0) = P(0) = 0, \quad m(0) = m_0 = \gamma/\lambda, \quad (9)$$

and the total mass of the system is conserved for all time $M_{\text{tot}}(t) = m_0$. The term ‘unseeded’ refers to the fact that, initially, there is no toxic protein in the system (hence, no seed). This condition assumes a lack of aggregated species in a healthy in vivo state. Indeed, it is observed that soluble $A\beta$ monomers are found in healthy individuals of all ages while aggregates larger than monomers are correlated with Alzheimer’s disease progression [17]. An extra advantage of this approach is that it fixes the constant $\gamma = m_0\lambda$.

Before we study the system in full generality, it is useful to consider the overall dynamic of the system for a typical set of parameters for the aggregation of $A\beta_{40}$ given in the first column of Table 1. We will use this set of parameters for all our examples. The other data sets are qualitatively equivalent and the values of various derived quantities are given in Table 1. As shown in Fig. 2, the typical behavior of the system from an unseeded initial condition is for the toxic protein mass to increase up to finite value M_∞ while the monomer concentration decreases to m_∞ in a typical sigmoid-like behavior. We observe that, in the absence of clearance, the monomer population is

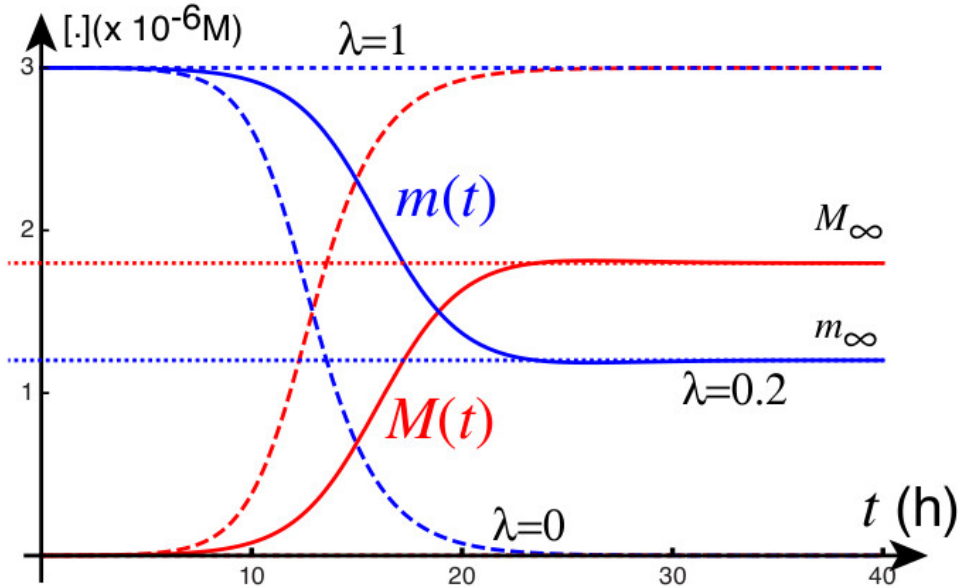


Figure 2: Typical dynamics of the monomer (blue) and toxic (red) concentration (in moles) for different values of the clearance (λ in h^{-1}) for $A\beta_{40}$ with parameters from Table 1 and $\lambda = 0$ (large dashed), $\lambda = 0.2$ (solid) and $\lambda = 1$ (small dashed). Asymptotic values for $\lambda = 0.2$ are shown with dotted lines.

completely converted to toxic proteins ($\lambda = 0$, dashed curves in Fig. 2). Conversely, for large clearance almost no conversion takes place ($\lambda = 1$, dotted curves in Fig. 2). Some of the monomers are converted (solid curves for $\lambda = 0.2$ in Fig. 2) for the case of moderate clearance. Of particular interest for our discussion is the change of behavior at some critical value λ_{crit} of the clearance λ where aggregation becomes negligible.

To derive an exact value for λ_{crit} , we determine the dependence of the asymptotic states m_∞ on λ . Using the steady state hypothesis with $m = m_\infty$, $P = P_\infty$ and $M = M_\infty$ in (5)-(6) one expresses the latter two states as a function of the parameters, λ and m_∞ . These relations are substituted in (7) to produce the implicit equation $q(\lambda, m_\infty) = 0$ with

$$\begin{aligned}
q(m_\infty, \lambda) = & 2k_+k_n m_\infty^5 - m_\infty^4 (2k_+k_2 K_M - 2\lambda k_n + 2k_n k_{\text{off}}) \\
& - m_\infty^3 (-\lambda^2 - 2k_+k_2 m_0 K_M + 2k_2 \lambda K_M - 2k_+k_n K_M - 2k_2 k_{\text{off}} K_M - 2k_+k_0) \\
& - m_\infty^2 (-2k_0 \lambda - 2k_2 \lambda m_0 K_M + 2k_2 m_0 k_{\text{off}} K_M - 2\lambda k_n K_M + 2k_n k_{\text{off}} K_M + 2k_0 k_{\text{off}} + \lambda^2 m_0) \\
& + m_\infty (\lambda^2 K_M + 2k_+k_0 K_M) + 2\lambda k_0 K_M - 2k_0 k_{\text{off}} K_M - \lambda^2 m_0 K_M
\end{aligned} \tag{10}$$

For instance, for the same parameter values as in Fig. 2, we show in Fig. 3 the values of m_∞ as a function of λ . We observe a sharp transition for a critical value of the clearance parameter λ .

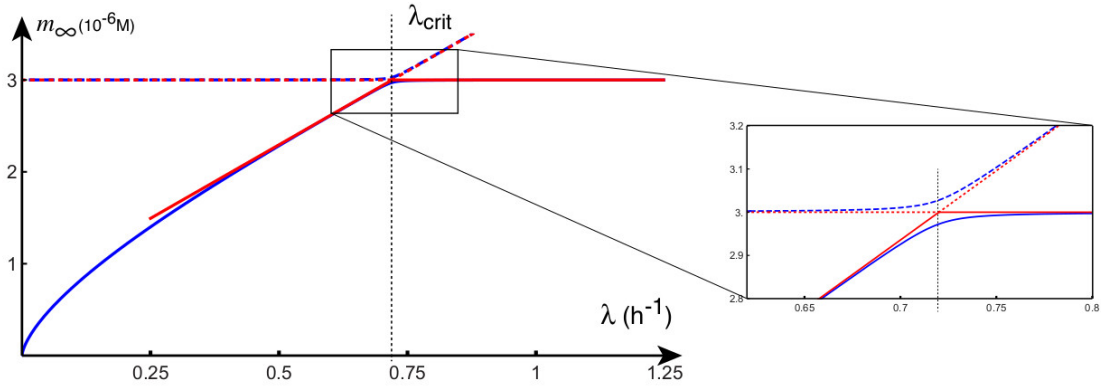


Figure 3: Perfect (red) and imperfect (blue) transcritical bifurcation obtained for A β 40. Unstable (dashed) and stable (solid) equilibrium solutions. In this case, we have $\tilde{\lambda}_{\text{crit}} \approx 0.72$ and $\tilde{m}_\infty \approx 0.7 + 3.2\tilde{\lambda}$. Dashed curves indicate unstable equilibria solutions and solid curves denote stable equilibria.

There are three necessary conditions for λ_{crit} : first that λ_{crit} is non-negative; second that m_∞ is maximal; and third that the value of m_∞ coincides with m_0 . The last two conditions can be realized by computing the derivative of the expression $q(\lambda, m_\infty) = 0$ evaluated at $m = m_\infty$. Therefore, λ_{crit} is given by the positive root of $L(\lambda) = 0$ where

$$\begin{aligned}
L(\lambda) = & \left. \frac{\partial q}{\partial m_\infty} \right|_{m_\infty=m_0} \\
= & -4k_{\text{off}} K_M m_\infty (k_2 m_0 + k_n) + 6k_+k_n K_M m_\infty^2 + 6k_2 k_{\text{off}} K_M m_\infty^2 - 8k_+k_2 K_M m_\infty^3 \\
& + 6k_+k_2 m_0 K_M m_\infty^2 + 2k_+k_0 K_M - 8k_n k_{\text{off}} m_\infty^3 + 10k_+k_n m_\infty^4 - 4k_0 k_{\text{off}} m_\infty + 6k_+k_0 m_\infty^2 \\
& + \lambda (4K_M m_\infty (k_2 m_0 + k_n) - 6k_2 K_M m_\infty^2 + 8k_n m_\infty^3 + 4k_0 m_\infty) + \lambda^2 (K_M + 3m_\infty^2 - 2m_0 m_\infty)
\end{aligned} \tag{11}$$

For A β -40 the critical clearance, as shown in Fig. 3, is $\lambda_{\text{crit}} = 0.72$. Critical clearance rates for the other experimental data sets are given in Table 1 for comparison.

3.2 Bifurcation and normal form analysis

In a neighborhood of λ_{crit} , m_∞ , as a function of λ , undergoes a sharp transition. This transition is not a bifurcation in the strict sense but, in the parlance of dynamical systems, it can be described as an imperfect transcritical bifurcation when heterogeneous nucleation and homogeneous nucleation terms can be understood as an imperfection and are sufficiently small with respect to the elongation. More specifically, when $k_0/(k_+m_0^2) \ll 1$ and $k_n/k_+ \ll 1$ the system is well approximated by $k_0 = 0$ and $k_n = 0$. In this limiting case, the fixed point $(P, M, m) = (0, 0, m_0)$ for the system (5)-(7) undergoes a (perfect) transcritical bifurcation at $\tilde{\lambda}_{\text{crit}} \approx \lambda_{\text{crit}}$ that can be obtained by locally expanding m_∞ in λ to find

$$\tilde{m}_\infty = m_0 + \frac{1}{\alpha}(\lambda - \tilde{\lambda}_{\text{crit}}) + \mathcal{O}\left((\lambda - \tilde{\lambda}_{\text{crit}})^2\right), \quad (12)$$

where $\tilde{\lambda}_{\text{crit}}$ is specified by the formula

$$\tilde{\lambda}_{\text{crit}} = \frac{m_0 \left(\sqrt{k_2 K_M (m_0 (k_2 m_0 + 2k_+) K_M - 2k_{\text{off}} K_M + 2m_0^2 (k_+ m_0 - k_{\text{off}})) + k_2 m_0 K_M} \right)}{K_M + m_0^2}, \quad (13)$$

and α is defined by the expression

$$\alpha = \frac{m_0 \left(k_2 K_M \left(2\tilde{\lambda}_{\text{crit}} + 3k_+ m_0 - 2k_{\text{off}} \right) - \tilde{\lambda}_{\text{crit}}^2 \right)}{\tilde{\lambda}_{\text{crit}} (K_M + m_0^2) - k_2 m_0^2 K_M}. \quad (14)$$

When the clearance is close to the critical value the linear approximation to the perfect bifurcation is a reasonable approximation for the imperfect bifurcation as can be appreciated in Fig. 3 where $\tilde{\lambda}_{\text{crit}} \approx 0.72$ and $\tilde{m}_\infty \approx 0.7 + 3.2\tilde{\lambda}$. By analogy with epidemiology we define a dimensionless *neurodegenerative reproduction number*

$$R_0 = \frac{\tilde{\lambda}_{\text{crit}}}{\lambda}, \quad (15)$$

such that for $R_0 < 1$ the protein toxic level is negligible and grows to finite value for $R_0 > 1$.

The existence of a critical clearance rate shows that in the healthy regime, i.e. for sufficiently large values of clearance, the system (1)-(3) with size-independent clearance can support a small, endemic, population of toxic proteins. The aggregation of a significant toxic population, in this case, occurs only when the system's clearance rate, λ , drops sufficiently below the critical clearance rate λ_{crit} . We can explore the dynamics close to the bifurcation by considering the normal form of the system for the perfect system ((5)-(7) with $k_0 = k_n = 0$) near $\lambda = \tilde{\lambda}_{\text{crit}}$. The general method to obtain the normal form of a transcritical bifurcation for an arbitrary smooth vector field is given in Appendix A. Applying these ideas, we can approximate the full system by

$$\dot{P} = -(\lambda - \tilde{\lambda}_{\text{crit}})P + \frac{\alpha}{v_P}P^2, \quad (16)$$

$$\dot{M} = -(\lambda - \tilde{\lambda}_{\text{crit}})M - \alpha M^2, \quad (17)$$

$$\dot{m} = -(\lambda - \lambda_{\text{crit}})(m - m_0) + \alpha(m - m_0)^2, \quad (18)$$

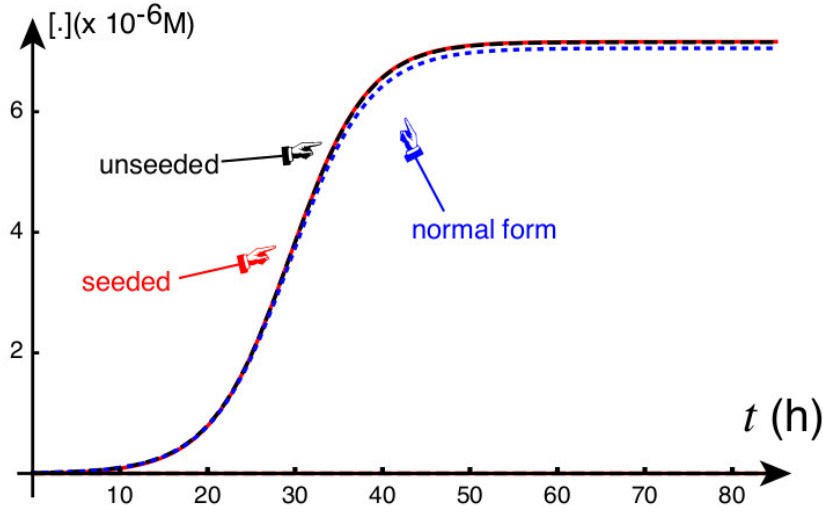


Figure 4: Toxic mass concentration $M(t)$ as a function of time for the unseeded (black dashed) system (5)-(7), for the perfect seeded system (neglecting homogeneous and heterogeneous primary nucleation) (red) and the normal form approximation of $M(t)$ (dotted blue). The initial conditions were selected so that the initial growth rates matched the initial growth rate of the unseeded system. Taking $S = 2.4 \times 10^{-13}$ to be a small seed value, the red curve was generated with unseeded initial conditions; the black dashed curve was computed using seeded initial conditions given by $(P(0), M(0), m(0)) = (S, S/2, m_0 - S)$; and, the blue dashed curve was generated by solving (17) with $M(0) = S/2$. Parameters are for the A β 40 values of Table 1 and $\lambda = 1/2$.

where α is given by (14) and

$$v_P = -\frac{\tilde{\lambda}_{\text{crit}}}{2(k_+ m_0 - k_{\text{off}} + \tilde{\lambda}_{\text{crit}})}. \quad (19)$$

Fig. 4 shows a comparison of the total toxic mass evolution, versus time, obtained for the imperfect unseeded system, the perfect seeded system, and the normal form. As expected, the agreement is excellent as long as the system is close enough to the bifurcation point.

3.3 Size distribution

Next, we consider the effect of clearance on size distribution. First, we take $k_{\text{off}} = 0$ as suggested by the data sets. Since, we are interested in the asymptotic size distribution, we can assume that $p_1 = m_\infty$ in Eqs. (1-3), in which case, we have simply that

$$p_i = \frac{2k_+ m_\infty}{\lambda + 2k_+ m_\infty} p_{i-1} = \delta_0 p_{i-1}, \quad \Rightarrow \quad p_i = \delta_0^{i-2} p_2, \quad i > 2. \quad (20)$$

Using the definition of $M = \sum_{i>1} i p_i$, we obtain:

$$p_2 = M_\infty \frac{(1 - \delta_0)^2}{2 - \delta_0}, \quad \Rightarrow \quad p_i = M_\infty \frac{\delta_0^{i-2} (1 - \delta_0)^2}{2 - \delta_0} \quad i > 2. \quad (21)$$

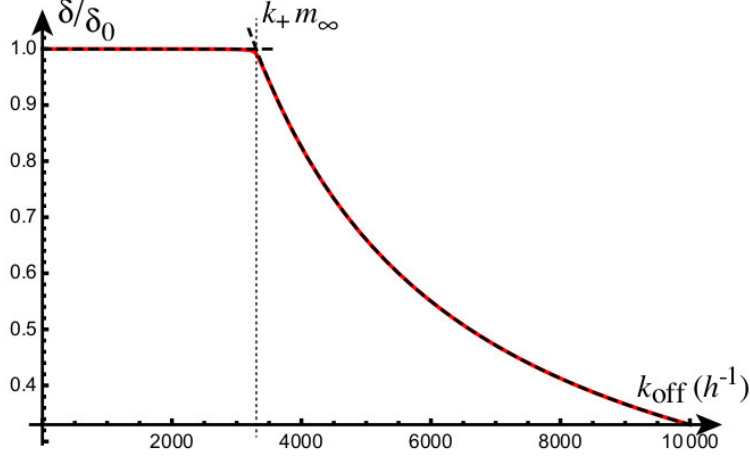


Figure 5: The effect of the parameter k_{off} on the size distribution can be appreciated by computing δ/δ_0 as a function of k_{off} . We see that for $k_{\text{off}} < m_{\infty}k_+$, the role of k_{off} is negligible. The dashed curves are given by the asymptotic approximation (25). Parameters are for the A β 40 values of Table 1 and $\lambda = 1/2$.

This analysis is not valid for $\lambda \rightarrow 0$. In that case, the total mass of the system is systematically transferred to larger and larger particles and in the long-time limit all finite aggregate concentrations tend to vanish and the trivial distribution is $p_i = p_{i-1} = p_2 = 0$. However, in that limit, the assumption $k_{\text{off}} = 0$ is not justified anymore as even a small value of k_{off} allows for a non-trivial size distribution. Indeed, with $k_{\text{off}} \neq 0$, we have the following recurrence relation for c_i

$$0 = -\lambda_i p_i + 2k_+ m_{\infty} (p_{i-1} - p_i) + 2k_{\text{off}} (p_{i+1} - p_i), \quad i > 2, \quad (22)$$

with a single bounded solution for the form

$$p_i = \delta^{i-2} p_2, \quad i > 2. \quad (23)$$

with

$$\delta = \frac{k_+ m_{\infty}}{2k_{\text{off}}} + \frac{1}{2} + \frac{\lambda}{4k_{\text{off}}} - \frac{1}{2} \sqrt{\frac{(2k_{\text{off}} + 2k_+ m_{\infty} + \lambda)^2}{4k_{\text{off}}^2} - \frac{4k_+ m_{\infty}}{k_{\text{off}}}}. \quad (24)$$

An asymptotic expression of δ for small and large values of k_{off} gives:

$$\delta = \begin{cases} \delta_0 \left(1 - \frac{2\lambda k_{\text{off}}}{(2m_{\infty}k_+ + \lambda)^2}\right) + \mathcal{O}(k_{\text{off}}^2), & \text{for } k_{\text{off}} < m_{\infty}k_+, \\ \delta_0 \frac{2m_{\infty}k_+ + \lambda}{2k_{\text{off}}} + \mathcal{O}(k_{\text{off}}^{-2}), & \text{for } k_{\text{off}} > m_{\infty}k_+. \end{cases} \quad (25)$$

We see that unless $\lambda = 0$, the role of k_{off} , when sufficiently small, is negligible. We conclude that clearance (or depolymerization) is sufficient to obtain a non-degenerate size distribution.

4 Size-dependent clearance

Next, we assume that clearance of an aggregate depends on its size. In this case, there is no simple, closed equation for the moments, as in Sec. 3, and we must study the full system. Here, we make a

key assumption about the dependence of the clearance on the aggregate size. We assume that there exists a critical aggregate size, N , such that all aggregates of size N , or greater, are too large to be cleared. Explicitly, this assumption implies that $\lambda_i = 0, \forall i \geq N$. We also assume that $k_{\text{off}} = 0$ and $n_c = n_2 = 2$ then (1)-(3) can be written

$$\frac{d\tilde{M}}{dt} = - \sum_{i=2}^{N-1} \lambda_i i p_i + 2k_0 + 2k_n p_1^2 + 2k_+ p_1 P + 2k_2 \sigma(p_1) \tilde{M}, \quad (26)$$

$$\frac{dp_1}{dt} = \lambda_1(m_0 - p_1) - 2k_0 - 2k_n p_1^2 - 2k_+ p_1 P - 2k_2 \sigma(p_1) \tilde{M}, \quad (27)$$

$$\frac{dp_2}{dt} = -\lambda_2 p_2 + k_0 + k_n p_1^2 - 2k_+ p_1 p_2 + k_2 \sigma(p_1) \tilde{M}, \quad (28)$$

$$\frac{dp_i}{dt} = -\lambda_i p_i + 2k_+ p_1 (p_{i-1} - p_i). \quad i > 2, \quad (29)$$

where $P = \sum_{i=2}^{\infty} p_i$ and $\tilde{M} = \sum_{i=2}^{\infty} i p_i$. The unseeded initial conditions for this system are

$$p_1(0) = m_0, \quad p_i(0) = 0 \text{ for } 2 \leq i, \quad \tilde{M}(0) = 0. \quad (30)$$

In general, there is no guarantee of mass conservation. For instance, if $\lambda_i \leq \lambda_1 \forall i > 2$ and there is at least one $i \geq 2$ such that $\lambda_i < \lambda_1$, then the overall mass of proteins will increase in time as shown in Appendix B.

4.1 A finite super-particle system

To study the dynamics of (26)-(29), we introduce a finite system with equivalent dynamics. Here, we follow [19] (see also [20]) and introduce a super-particle, denoted q_N , which represents the concentration of all aggregates of size greater than or equal to N :

$$q_N = \sum_{i=N}^{\infty} p_i, \quad (31)$$

Since $\lambda_i = 0$ for all $i \geq N$; we can take the limit of the partial sums of (29) to obtain

$$\frac{dq_N}{dt} = \sum_{i=N}^{\infty} 2k_+ p_1 (p_{i-1} - p_i) = \lim_{j \rightarrow \infty} \sum_{i=N}^j 2k_+ p_1 (p_{i-1} - p_i) = 2k_+ p_1 p_{N-1} - 2k_+ \lim_{j \rightarrow \infty} p_1 p_j. \quad (32)$$

Since the monomer concentration p_1 , remains bounded, for any fixed time, the last term of (32) tends to zero as $j \rightarrow \infty$ and the super particle concentration satisfies the equation

$$\frac{dq_N}{dt} = 2k_+ p_1 p_{N-1}. \quad (33)$$

We will distinguish the *finite* system with a super-particle from the *infinite* system (26)-(29) by introducing the notation $q_i = p_i$ for $i < N$. Defining $Q = \sum_{i=2}^N q_i$, and using (33), the corresponding

super-particle system is defined by

$$\frac{dM}{dt} = - \sum_{i=2}^{N-1} \lambda_i i q_i + 2k_0 + 2k_n m^2 + 2k_+ m Q + 2k_2 \sigma(m) M, \quad (34)$$

$$\frac{dm}{dt} = \lambda_1(m_0 - m) - 2k_0 - 2k_n m^2 - 2k_+ m Q - 2k_2 \sigma(m) M, \quad (35)$$

$$\frac{dq_2}{dt} = -\lambda_2 q_2 + k_0 + k_n m^2 - 2k_+ m q_2 + k_2 \sigma(m) M, \quad (36)$$

$$\frac{dq_i}{dt} = -\lambda_i q_i + 2k_+ m (q_{i-1} - q_i), \quad i = 2, \dots, N-1, \quad (37)$$

$$\frac{dq_N}{dt} = 2k_+ m q_{N-1}. \quad (38)$$

The unseeded conditions for (34)-(38) are

$$m(0) = m_0, \quad q_i(0) = 0, \text{ for } 2 \leq i \leq N, \quad M(0) = 0. \quad (39)$$

For unseeded initial conditions, the dynamics of the finite system is equivalent to the infinite one in the following sense: First note that $\dot{Q} = \dot{P}$; this follows directly from the definition of Q , P and (31). Thus, Q and P will agree, for all time. In turn, (26) and (34) coincide when the initial data (30) and (39), respectively, are used; thus $\tilde{M}(t) = M(t)$ in this case. Finally, by definition, $p_i = q_i$ for $2 \leq i < N$ and (31)-(32) has already established that solving (38) produces $q_N(t) = \sum_{i=N}^{\infty} p_i(t)$ provided the initial conditions agree. The above establishes an important fact that we rely on for the rest of the section; solving (26)-(29) with initial conditions (30) and solving (34)-(38) with initial conditions (39) yields

$$m(t) = p_1(t), \quad Q(t) = P(t), \quad M(t) = \tilde{M}(t), \quad (40)$$

$$p_i(t) = q_i(t) \text{ for } 2 \leq i < N \quad \text{and} \quad q_N(t) = \sum_{i=1}^{\infty} p_i(t).$$

We remark, however, that $M(t)$, defined as the solution of (34), is the total toxic mass of both (26)-(29) and (34)-(38), due to (40), for the unseeded initial conditions (39); however, $M(t)$ cannot be constructed a posteriori from the knowledge of $q_i(t)$ where $i = 2, 3, \dots, N$ in the same manner that $\tilde{M}(t)$ can be retrieved from the knowledge of the $p_i(t)$. That is, we have $M(t) \neq \sum_{i=2}^N i q_i(t)$. Indeed, in the closure process of reducing the full system to a finite one, we lost information regarding the mass of individual particles making up the superparticle. Nevertheless, both the evolution of toxic mass of the full system, as well as the size distribution (up to size N) can be obtained by studying the finite system (34)-(38).

4.2 Toxic mass behaviour

Systems such as (26)-(29) or (34)-(38), with size-dependent clearances, do not conserve mass in general (see Appendix B) and the toxic mass may increase with time. We study in more details the particular choice

$$\lambda_i = \lambda/i, \quad \text{for } i = 1, 2, \dots, N-1, \quad (41)$$

which expresses the modeling assumption that aggregates become increasingly difficult to clear as their size increases. An example of the dynamics of the system (34)-(38) is shown in Fig. 6. We observe two different behaviors. Initially, up to a time τ_2 , the system mostly behaves like the conservative no-clearance model ($\lambda = 0$) even for large values of clearance. This behavior is markedly different than the one observed in Fig. 2. Second for larger times, $t > \tau_2$, the monomer mass always decreases and the toxic mass always increases as predicted from our general analysis. We observe that larger clearance leads to faster toxic mass creation. This is due to the fact that in healthy homeostasis, production and clearance are balanced. Hence larger clearance implies larger production. The question is then to understand the transition between the two regimes as well as the small and large time behaviors of all species.

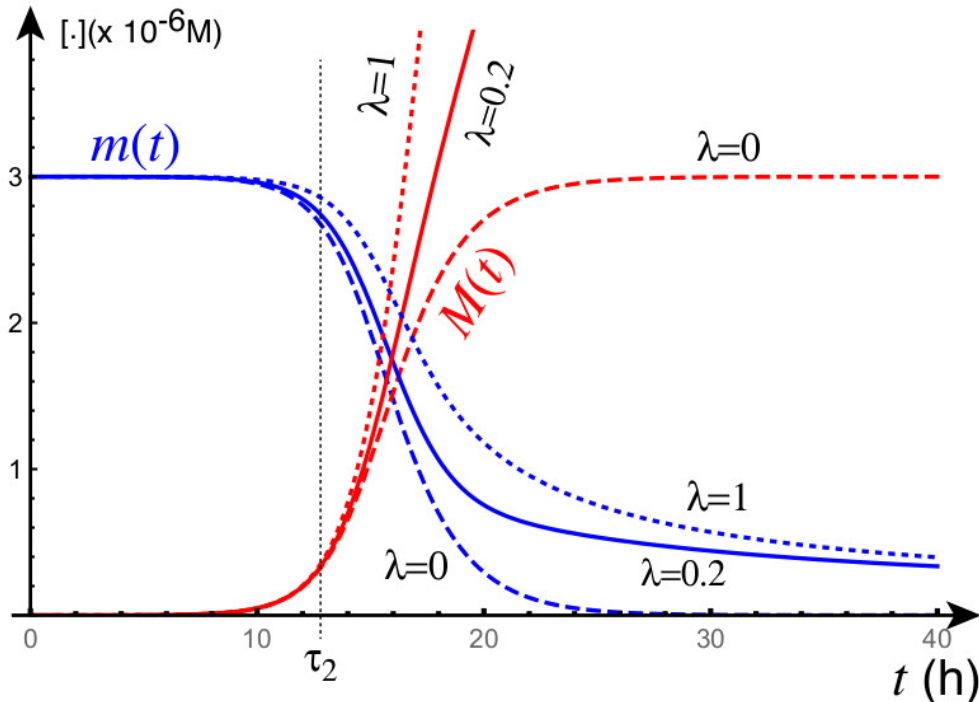


Figure 6: Toxic mass dynamics for the size-dependent clearance $\lambda_i = \lambda/i$; the monomer population concentration ($m(t)$, blue lines) and total toxic mass ($M(t)$, red lines) are shown for clearance (in h^{-1}) rates: $\lambda = 0$ (dashed), $\lambda = 0.2$ (solid), and $\lambda = 1$ (dotted). Parameters are for the A β 40 values of Table 1 and $\lambda = 1/2$ $N = 20$.

4.3 Long-time dynamics

On long time scales, i.e. long enough so that the monomer concentration begins to decrease, the monomer production, aggregation, and nucleation processes result in an increase to subsequent toxic species and, therefore, to the overall toxic mass M . The asymptotic behavior of the system toxic mass M is observed to depend entirely on the production rate, $\gamma = \lambda m_0$, as

$$M(t) \underset{t \rightarrow \infty}{\sim} \gamma t. \quad (42)$$

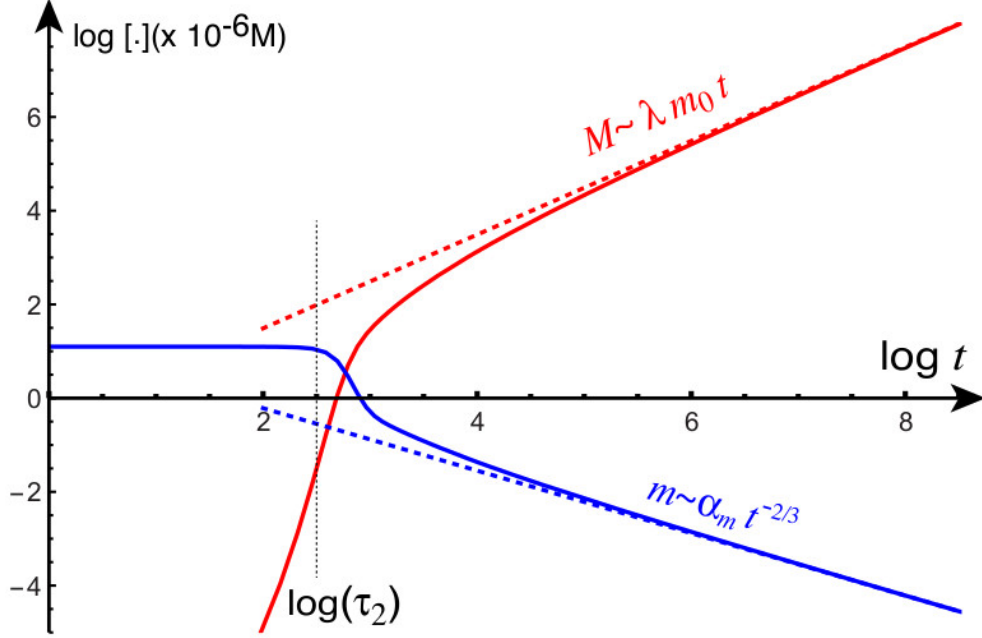


Figure 7: Long time (in h) concentration (in moles) dynamics of (34)-(38) ($\lambda_i = \lambda/i$, in h^{-1}) with $N = 20$ and A β 40 parameters (Table 1, third column); curves for $\lambda = 0.2$ (solid) with asymptotic slopes (dotted). Time runs from 0 to 5000 hours. Parameters are for the A β 40 values of Table 1 and $N = 20$.

This behavior is illustrated in a log-plot in Fig. 7; the characteristic time scale, τ_2 , indicates the time at which the monomer mass begins to decay. Once the asymptotic behavior of M has been established, the equations can be balanced asymptotically by the following dynamics:

$$m \sim \alpha_m t^{-2/3}, \quad q_N \sim \alpha_N t^{2/3}, \quad q_i \sim \alpha_i t^{1/3}, \quad i = 1, \dots, N-1, \quad (43)$$

where the symbol “ \sim ” is understood as the long-time asymptotic behavior and the α_i are constants. This asymptotic behavior shows that the super-particle dominates the long-term dynamics; thus $P \sim q_N$ for large times. Physically, in the long-time limit, the monomer population, renewed by the continuous production, is quickly promoted to the super-particle through linear aggregation.

4.4 Early-time dynamics

We observe in Fig. 6 that the early-time behavior is not greatly perturbed by altering the clearance rate. Hence, we can obtain characteristic time scales for the amplification of the toxic mass by considering the limit $\lambda \rightarrow 0^+$. In this case, the early evolution of the toxic mass is governed by the dynamics of (5)-(7) with $\lambda = 0$. There are two characteristic time scales of importance. First, the time scale τ_1 associated with the exponential growth of the toxic mass in early time via the inverse of the positive linear eigenvalue, $\mu = 1/\tau_1$, corresponding to the linearization of (5)-(7) around the healthy state $m = m_0$, $M = P = 0$. The linear eigenvalue is given by the positive root of

$$\mu^2 + \mu \left(4m_0 k_n - \frac{2k_2 m_0^2 K_M}{K_M + m_0^2} \right) - \frac{2k_+ k_2 m_0^3 K_M}{K_M + m_0^2} + 4k_+ m_0^2 k_n = 0. \quad (44)$$

Second, there is a time scale τ_2 where both nucleation and amplification are balanced. It is given by the time for the linearized solution for $M(t)$ to reach m_0 . Hence τ_2 is the solution of

$$m_0^2 = \frac{(m_0^2 k_n + k_0)(K_M + m_0^2)}{2k_n K_M + 2m_0^2 k_n - k_2 m_0 K_M} \left(1 - \frac{e^{\tau_2/\tau_1}}{2}\right). \quad (45)$$

For example, for the first parameter set (A β 40) used for the figures, these times are $\tau_1 \approx 1.4$ h and $\tau_2 \approx 12.6$ h. The value of τ_2 is a rudimentary estimate for the time of amplification; it is a lower bound for the typical time scale of growth (see Fig. 6). Nevertheless, in Fig. 7, we see that τ_2 can indeed act as an indicator for the onset of decay for the monomer mass. A more refined estimate can be obtained by using the approximate solution for the full dynamics given in [12].

5 The case of a constant free monomer concentration

Another interesting case to consider is when the population of monomer is not depleted but remains at a constant level m_0 . We assume that, regardless of other parameters, that (1) is instead specified by

$$\frac{dp_1}{dt} = 0, \quad (46)$$

so that, with unseeded initial conditions, we have $p_1(t) = m_0$ for all time. Assuming again no depolymerization, no fragmentation, and dimer nucleation, the master equations now read

$$\frac{dp_2}{dt} = -\lambda_2 p_2 + k_0 + k_n m_0^2 - 2k_+ m_0 p_2 + k_2 \sigma_0 M, \quad (47)$$

$$\frac{dp_i}{dt} = -\lambda_i p_i + 2k_+ m_0 (p_{i-1} - p_i), \quad i > 2, \quad (48)$$

where $\sigma_0 = \sigma(m_0)$ and $M = \sum_{i=2}^{\infty} i p_i$ is the total toxic mass. This is an infinite system of linear ordinary differential equations. For this system, we consider three types of clearance; the size-independent case in addition to two different size-dependent paradigms. All three clearance relations can be summarily presented by a power-law of the form

$$\lambda_i = \lambda i^\nu. \quad (49)$$

When $\nu = 0$ we recover the size-independent case; when $\nu = -1$ we recover the size-dependent diminishing clearance formulation used in Sec. 4; and, finally, the case of $\nu = 1$ corresponds to improved clearance, with increasing size, which could arise due to, for instance, antibody binding. Depending on the two parameters λ and ν , the solution to this system may have a steady state or increase indefinitely. The question is then to identify the critical values at which this transition happens.

5.1 A constant free monomer population with constant clearance

We start with the simple case of constant clearance $\nu = 0$; this is the analogue to Sec. 3 for a constant free monomer assumption (c.f. (46)) The moments (c.f. Sec 3) are specified by a simple

pair of linear equations given by

$$\frac{dP}{dt} = -\lambda P + k_0 + k_n m_0^2 + k_2 \sigma_0 M, \quad (50)$$

$$\frac{dM}{dt} = -\lambda M + 2k_0 + 2k_+ m P + 2k_n m_0^2 + 2k_2 \sigma_0 M, \quad (51)$$

which can be written as

$$\dot{\mathbf{q}} = A\mathbf{q} + \mathbf{b}, \quad (52)$$

where $\mathbf{q} = (P, M)^T$, $\mathbf{b} = (k_0 + k_n m_0^2, 2k_0 + 2k_n m_0^2)^T$ and

$$A = \begin{pmatrix} -\lambda & a \\ b & 2a - \lambda \end{pmatrix} = \begin{pmatrix} -\lambda & k_2 \sigma_0 \\ 2k_+ m_0 & 2k_2 \sigma_0 - \lambda \end{pmatrix}. \quad (53)$$

The constant solution sole steady state for this system is $\mathbf{q}_\infty = -A^{-1}\mathbf{b}$; \mathbf{q}_∞ is positive and finite if

$$\lambda > a + \sqrt{a^2 + ab} = k_2 \sigma_0 + \sqrt{k_2^2 \sigma_0^2 + 2k_2 \sigma_0 k_+ m_0} = \lambda_{\text{crit}}^{(0)}. \quad (54)$$

This condition naturally provides a value for the critical clearance. Specifically, the largest linear eigenvalue for the system is $\kappa = \lambda_{\text{crit}}^{(0)} - \lambda$; solutions converge to \mathbf{q}_∞ exponentially in time (as $e^{\kappa t}$) for $\lambda > \lambda_{\text{crit}}^{(0)}$ and grow unbounded for $\lambda \leq \lambda_{\text{crit}}^{(0)}$. The values given in Table 1 for the different parameters show that this estimate is indistinguishable from the case studied in Section 3, which is explained by the fact that at the bifurcation point, the monomer population is constant in both cases.

5.2 A constant free monomer population with non-constant clearance

We now turn our attention to the general case where the clearance terms are not constant. Then, the master equations do not yield a closed system for the moments. Nevertheless, due to the simplicity introduced by $p_1(t) = m_0$ being constant, we can find conditions for the existence of a fixed-point solution, (p_2^*, p_3^*, \dots) to (47)-(48). If such a steady state p_i^* for $i > 2$, exists, it must satisfy the recurrence relation

$$p_i^* = \delta_i p_{i-1}^*, \quad \delta_i = \frac{b}{b + \lambda_i} = \frac{2k_+ m_0}{2k_+ m_0 + \lambda_i}. \quad (55)$$

we note that each of the recursion coefficients, δ_i , is now dependent on i via λ_i . Define a sequence of real numbers, indexed by i , as

$$\Delta_i = \prod_{j=3}^i \delta_j, \quad i > 2. \quad (56)$$

We define $\Delta_2 = 1$ and the i^{th} steady state is expressible, for all $i \geq 2$, through its recurrence relation as

$$p_i^* = \Delta_i p_2^*, \quad i \geq 2. \quad (57)$$

Defining

$$\Delta = \sum_{j=3}^{\infty} \Delta_j, \quad (58)$$

the steady state for the total toxic mass solution M^* is then given by

$$M^* = \sum_{i=2}^{\infty} i \Delta_i p_2^* = \Delta p_2^*, \quad (59)$$

and an application of (47), at steady state, gives the value of p_2^* as

$$p_2^* = \frac{k_0 + k_n m_0^2}{\lambda_2 + 2k_+ m_0 - k_2 \sigma_0 \Delta}. \quad (60)$$

Therefore, for a fixed point to exist we need the three following conditions to be satisfied

$$\text{C1: } \lim_{i \rightarrow \infty} \Delta_i = 0, \quad (61)$$

$$\text{C2: } \Delta = \sum_{i=2}^{\infty} i \Delta_i \text{ converges,} \quad (62)$$

$$\text{C3: } k_2 \sigma_0 \Delta - \lambda_2 - 2k_+ m_0 > 0. \quad (63)$$

An analysis of the case $\nu = 0$ recovers the previous condition and it can then be verified directly that conditions C1-C3 are satisfied, as expected, for $\lambda > \lambda_{\text{crit}}^{(0)}$.

5.2.1 Enhanced clearance: $\nu = 1$

For $\nu = 1$, we have (see Appendix C), $\Delta^{(1)} = 2 + b/\lambda$ and the steady population of dimers, whenever it exists, is given by

$$p_2^* = \frac{\lambda(k_0 - k_n m_0^2)}{2(k_+ m_0 + \lambda)(\lambda - k_2 \sigma_0)}. \quad (64)$$

Hence, condition C3 leads to $\lambda > \lambda_{\text{crit}}^{(1)}$ with

$$\lambda_{\text{crit}}^{(1)} = k_2 \sigma_0. \quad (65)$$

We note that the above implies that the critical clearance depends only on the secondary nucleation process and, in particular, not the process of elongation (c.f. $\lambda_{\text{crit}}^{(0)}$ in (54)).

5.2.2 Reduced clearance: $\nu = -1$

For $\nu = -1$, the situation is not as simple. The condition C1 is verified but C2 leads to $\lambda > 2b$ for which

$$\Delta^{(-1)} = \frac{(\lambda + 2b) \left(\Gamma\left(\frac{\lambda}{b} - 2\right) \Gamma\left(\frac{\lambda}{b} + 2\right) - \Gamma\left(\frac{\lambda}{b}\right)^2 \right)}{2b \Gamma\left(\frac{\lambda}{b}\right)^2}, \quad (66)$$

where $\Gamma(\cdot)$ is the usual Gamma function. Condition C3 is satisfied if $\lambda > \lambda_{\text{crit}}^{(-1)}$ where $\lambda_{\text{crit}}^{(-1)}$ is the positive solution of

$$f\left(\frac{\lambda}{b}\right) = 1 + \frac{2k_+ m_0}{k_2 \sigma_0}, \quad \text{with} \quad f\left(\frac{\lambda}{b}\right) = \frac{\Gamma\left(\frac{\lambda}{b} - 2\right) \Gamma\left(\frac{\lambda}{b} + 2\right)}{\Gamma\left(\frac{\lambda}{b}\right)^2}. \quad (67)$$

This equation always has a solution as $f : z \in [2, \infty] \rightarrow f(z)$ is such that $f'(z) < 0$, $f(z) \rightarrow_{z \rightarrow 2} \infty$ and $f(z) \rightarrow_{z \rightarrow \infty} 1$. For the parameters listed in Table 1, $2k_+m_0/k_2\sigma_0 \gg 1$, in which case, we can approximate the function $f(z)$ close to $z = 2$ by $f(z) \approx 6/(z - 2)$, which leads to the critical value

$$\lambda_{\text{crit}}^{(-1)} = \frac{8k_+m_0(2k_2\sigma_0 + k_+m_0)}{k_2\sigma_0 + 2k_+m_0} \quad (68)$$

This last relation can be further simplified by realizing that $k_+m_0 \gg k_2\sigma_0$, which leads to

$$\lambda_{\text{crit}}^{(-1)} = 4k_+m_0. \quad (69)$$

For the parameters given in Table 1, this last approximation of the critical clearance gives the correct value (compared to (67)) to 6 digits. Note that, in contrast to the critical clearance rate for enhanced clearance (c.f. (65)), (68) depends only on the elongation rate k_+ . In particular, in a reduced clearance regime, a change in the rate of secondary nucleation has no effect on the clearance rate required to keep the system stable. The general trend that can be observed from Table 1 is that $\lambda_{\text{crit}}^{(-1)} > \lambda_{\text{crit}}^{(0)} > \lambda_{\text{crit}}^{(1)}$, as expected.

5.2.3 Further reduced clearance: $\nu = -2$

Finally, for $\nu = -2$, skipping computational details, we find that

$$\lim_{n \rightarrow \infty} \Delta_n^{(-2)} = \frac{1}{4} \pi \sqrt{\frac{\lambda}{b}} \left(\left(\frac{\lambda}{b} \right)^2 + 5 \frac{\lambda}{b} + 4 \right) \text{csch} \left(\pi \sqrt{\frac{\lambda}{b}} \right), \quad (70)$$

which is positive for all finite positive value of λ . Hence, condition C1 is not satisfied and there is no constant solution or critical value of the clearance that would limit unbounded growth of toxic proteins. We note that we have neglected the effect of fragmentation. For $\nu < 0$, the effect of fragmentation is the creation of smaller aggregates that increase the overall expansion of the protein population but also boosts clearance. Indeed since smaller aggregates are more likely to be cleared and we expect a reduction of the critical value of clearance as well as the possibility of a finite value of clearance for $\nu = -2$ or smaller as shown in Meisl [27]. Comparing the different critical clearance values given in Table 1 for the three values of ν , it is clear that the choice of clearance law has a significant impact on the clearance values as they differ, from the smallest to the largest by 9 orders of magnitude. Hence, enhancing or inhibiting the clearance mechanism may be extremely important to the overall increase of toxic proteins.

6 Conclusion

We have assessed the impacts of production and clearance on the aggregation kinetics using a theoretical model, c.f. (1)-(3), that has been experimentally validated [8, 15, 16]. Our findings suggest that clearance may mediate toxic aggregation kinetics. In the case of constant clearance, we showed that toxic aggregation is controlled, directly, by a critical clearance. Clearance above this level provides for a robust environment which is, essentially, free of toxic proteins; clearance below this level triggers and instability and a propensity towards toxic mass accumulation. Once toxic aggregation is triggered, the healthy monomer population is diminished as aggregates form. The

maximal amount of toxic formation is, again, mediated by the clearance level; an effect of the mass conservation principle, of this regime.

A reasonable *in vivo* hypothesis is that the clearance may depend on the aggregates size i . This clearance paradigm has been explored using a simple inverse proportionality law $\lambda_i = \lambda/i$. The resulting set of equations, for this type of clearance, does not yield a finite system for the moments; thus, a super-particle system, with identical trajectories in the presence of unseeded initial conditions, has been advanced as a means of study. In the presence of any aggregation effects, the system immediately begins accumulating toxic mass; even from unseeded initial conditions. Moreover, mass is not conserved and the toxic mass grows unboundedly in time. The clearance, however, determines the asymptotic rate of increase of the toxic mass as a function of time with $M(t) \sim \lambda m_0 t$. The biological implications of a size-dependent clearance are quite different than the constant case. In particular, if clearance is size-dependent, results suggest that we have no recourse in halting aggregate pathology through enhancing clearance; rather, we can only hope to delay the overall trend of toxic accumulation.

The theoretical model of a constant free-monomer concentration was also considered. This case is particularly interesting since, under the assumption of steady states, we see that a notion of critical clearance can be established for relations of the form $\lambda_i = \lambda i^\nu$ for $\nu \in \{-1, 0, 1\}$. In the case of $\nu = 0$, we recover the previous results given for constant clearance. Similarly, in the size-dependent case ($\nu = -1$ and $\nu = 1$), there exists a critical value of the clearance so that no aggregation takes place past that value. Remarkably, our results suggest that, depending on the specific size-dependence, the processes of elongation and secondary nucleation contribute to the value of the critical clearance to different degrees. An important implication is that, depending on the specific mechanism of clearance, inhibition of aggregation should target different processes in order to reduce the critical clearance rate.

Overall, the role of clearance in aggregation kinetics is highly non-trivial. However, our study shows that clearance may play an important role in the aggregation kinetics of Amyloid- β and that additional experiments, providing fitted values for clearance parameters, would serve to elucidate appropriate regimes for further study.

Acknowledgments— This work was supported by the Engineering and Physical Sciences Research Council grant EP/R020205/1 to Alain Goriely and by the John Fell Oxford University Press Research Fund grant 000872 (project code BKD00160) to Travis Thompson.

A Normal form for a transcritical bifurcation

Here we derive the normal form of a transcritical for a general dynamical system. We consider an autonomous n -dimensional \mathcal{C}^2 vector field of the form

$$\dot{\mathbf{x}} = \mathbf{f}(\mathbf{x}, \lambda), \quad \mathbf{x} \in \mathbb{R}^n, \quad (71)$$

and assume that there exists a constant solution \mathbf{x}_0 such that $\mathbf{f}(\mathbf{x}_0, \lambda) = \mathbf{0}$ and a different equilibrium solution in a neighborhood of the critical value λ_0 . The conditions for the existence of a transcritical bifurcation at the critical value λ_0 are given by Sotomayor's theorem [21] and the reduced form the system takes close to that value can be captured by normal form theory [22, 23, 24, 25]. Here, we use multiple scale analysis to obtain a convenient form of the reduced equations. The result in itself

is not original but it may not be obvious to find a direct reference for either the statement or the proof. Therefore, its inclusion may be helpful to the reader.

Using multiple-scale expansion, we expand the solution as

$$\mathbf{x} = \mathbf{x}_0 + \epsilon \mathbf{x}_1 + \epsilon^2 \mathbf{x}_2 + \dots, \quad \lambda = \lambda_0 + \epsilon \lambda_1. \quad (72)$$

where \mathbf{x}_0 is constant and $\mathbf{x}_i = \mathbf{x}_i(t, \tau)$, $i > 1$ and $\tau = \epsilon t$ is a slow time [26]. The expansion of the vector field close to second order is

$$f = \mathbf{f}_0 \quad (73)$$

$$+ \epsilon [D\mathbf{f}_0 \cdot \mathbf{x}_1 + \mathbf{f}_{\lambda,0} \lambda_1] \quad (74)$$

$$+ \epsilon^2 \left[D\mathbf{f}_0 \cdot \mathbf{x}_2 + \frac{1}{2} H\mathbf{f}_0(\mathbf{x}_1, \mathbf{x}_1) + \lambda_1 D\mathbf{f}_{\lambda,0} \cdot \mathbf{x}_1 \right] \quad (75)$$

$$+ \dots, \quad (76)$$

where $\mathbf{f}_0 = \mathbf{f}(\mathbf{x}_0, \lambda_0)$ indicates that \mathbf{f} is evaluated at the point $(\mathbf{x}_0, \lambda_0)$ and

$$(D\mathbf{f})_{ij} = \frac{\partial f_i}{\partial x_j}, \quad D\mathbf{f}_0 = D\mathbf{f}(\mathbf{x}_0, \lambda_0), \quad (77)$$

$$\mathbf{f}_\lambda = \frac{\partial \mathbf{f}}{\partial \lambda}, \quad \mathbf{f}_{\lambda,0} = \mathbf{f}_\lambda(\mathbf{x}_0, \lambda_0), \quad (78)$$

$$(H\mathbf{f})_{ijk} = \frac{\partial^2 f_i}{\partial x_j \partial x_k}, \quad H\mathbf{f}_0 = H\mathbf{f}(\mathbf{x}_0, \lambda_0), \quad (79)$$

$$(D\mathbf{f}_\lambda)_{ij} = \frac{\partial^2 f_i}{\partial x_j \partial \lambda}, \quad D\mathbf{f}_{\lambda,0} = D\mathbf{f}_\lambda(\mathbf{x}_0, \lambda_0). \quad (80)$$

If the system has a bifurcation of co-dimension one at λ_0 then $D\mathbf{f}_0$ has rank $n - 1$ and the following vectors \mathbf{w} and \mathbf{v} given by

$$\mathbf{w} \cdot D\mathbf{f}_0 = \mathbf{0}, \quad D\mathbf{f}_0 \cdot \mathbf{v} = \mathbf{0}, \quad (81)$$

define the left and right null spaces of $D\mathbf{f}_0$. The generic condition for a transcritical bifurcation to occur is

$$\mathbf{w} \cdot \mathbf{f}_{\lambda,0} = 0. \quad (82)$$

To order $\mathcal{O}(\epsilon)$, the differential equation reads

$$\dot{\mathbf{x}}_1 = D\mathbf{f}_0 \cdot \mathbf{x}_1 + \lambda_1 \mathbf{f}_{\lambda,0}. \quad (83)$$

and we are interested in the solution

$$\mathbf{x}_1 = c(\tau) \mathbf{v}, \quad (84)$$

whose existence is guaranteed by the condition $\mathbf{w} \cdot \mathbf{f}_{\lambda,0} = 0$. To second order $\mathcal{O}(\epsilon^2)$, we have

$$\dot{\mathbf{x}}_2 + c'(\tau) \mathbf{v} = D\mathbf{f}_0 \cdot \mathbf{x}_2 + c^2 \frac{1}{2} H\mathbf{f}_0(\mathbf{v}, \mathbf{v}) + c \lambda_1 D\mathbf{f}_{\lambda,0} \cdot \mathbf{v}. \quad (85)$$

The Fredholm alternative gives a condition for the existence of a solution of this inhomogeneous system:

$$\mathbf{w} \cdot (c'(\tau) \mathbf{v}) = \mathbf{w} \cdot \left(c^2 \frac{1}{2} H\mathbf{f}_0(\mathbf{v}, \mathbf{v}) + c \lambda_1 D\mathbf{f}_{\lambda,0} \cdot \mathbf{v} \right), \quad (86)$$

which gives the equation

$$c'(\tau) = \beta\lambda_1 c + \alpha c^2, \quad (87)$$

where

$$\alpha = \frac{1}{2} \frac{1}{\mathbf{v} \cdot \mathbf{w}} \mathbf{w} \cdot H\mathbf{f}_0(\mathbf{v}, \mathbf{v}) \quad (88)$$

$$\beta = \frac{1}{\mathbf{v} \cdot \mathbf{w}} \mathbf{w} \cdot D\mathbf{f}_{\lambda,0} \cdot \mathbf{v}. \quad (89)$$

Taking into account that $\epsilon\lambda_1 = \lambda - \lambda_0$ and defining $y = \epsilon c$, the local solution is $\mathbf{x} = \mathbf{x}_0 + y\mathbf{v}$ where

$$\dot{y} = \beta(\lambda - \lambda_0)y + \alpha y^2, \quad (90)$$

is the normal form of a transcritical bifurcation at $\lambda = \lambda_0$. The local evolution of the variables for which $v_i \neq 0$ is given by

$$\dot{x}_i = \beta(\lambda - \lambda_0)(x_i - x_{0,i}) + \frac{\alpha}{v_i}(x_i - x_{0,i})^2. \quad (91)$$

B Mass balance in the size-dependent clearance case

For unseeded initial conditions, we can show that the total mass of the system is not conserved. Assume that, for all $2 \leq i$ we have $\lambda_i \leq \lambda_1$ and assume that there exists some index j , with $2 \leq j$, such that the inequality is strict (i.e. $\lambda_j < \lambda_1$). In this case we have

$$\begin{aligned} \frac{d\tilde{M}}{dt} &> -\lambda_1 \sum_{i=2}^{N-1} ip_i + 2k_0 + 2k_n p_1^2 + 2k_{+p_1} P + 2k_2 \sigma(p_1) \tilde{M} \\ &> -\lambda_1 \sum_{i=2}^{\infty} ip_i + 2k_0 + 2k_n p_1^2 + 2k_{+p_1} P + 2k_2 \sigma(p_1) \tilde{M} \\ &= -\lambda_1 \tilde{M} + 2k_0 + 2k_n p_1^2 + 2k_{+p_1} P + 2k_2 \sigma(p_1) \tilde{M}. \end{aligned} \quad (92)$$

Likewise for $i = 2$ we have a similar inequality

$$\begin{aligned} \frac{dp_2}{dt} &= -\lambda_2 p_2 + k_0 + k_n p_1^2 - 2k_{+p_1} p_2 + k_2 \sigma(p_1) \tilde{M}, \\ &> -\lambda_1 p_2 + k_0 + k_n p_1^2 - 2k_{+p_1} p_2 + k_2 \sigma(p_1) \tilde{M}, \end{aligned} \quad (93)$$

and likewise for $i > 2$. The above observation shows that the system (26)-(29) grows faster than the constant-clearance case system where $\lambda_i = \lambda_1$ for every $i \in \{1, 2, \dots\}$. We note that, as in Sec. 3, the total system mass for (26)-(29) is $\tilde{M}_{\text{tot}} = \tilde{M} + p_1$; this follows from the common definition of \tilde{M} , here, and M (see (4)). Adding (26) to (27) and using (92) gives

$$\frac{d\tilde{M}_{\text{tot}}}{dt} > \lambda_1 (m_0 - \tilde{M}_{\text{tot}}). \quad (94)$$

In the presence of the unseeded initial conditions (30) we have that $\tilde{M}_{\text{tot}}(0) = m_0$ so that the left-hand side of (94) is strictly positive and mass conservation is violated at the outset. Now let

$M_{\text{tot}}^{\lambda_1}$ denote the total mass of the constant clearance case $\lambda_i = \lambda_1$ for all i . We know that, in the presence of unseeded initial conditions, a sysetm with constant clearance systems conserves mass so that

$$\frac{dM_{\text{tot}}^{\lambda_1}}{dt} = 0.$$

From (92) and (93), which holds analogously for $i > 2$ and for $i = 1$ we have equality, we can conclude that

$$\frac{d\tilde{M}_{\text{tot}}}{dt} \geq \frac{dM_{\text{tot}}^{\lambda_1}}{dt} = 0, \quad (95)$$

for unseeded initial conditions. Take together, (94) implies that the system (26)-(29), with unseeded initial conditions, initially gains mass while (95) shows that it can never lose mass. Therefore, not only does (26)-(29) not conserve mass but it can never return to the state of initial unseeded mass.

C Critical value for enhanced clearance

For $\nu = 1$, the case (56) takes the form

$$\begin{aligned} \Delta_i &= \prod_{m=3}^i \left(\frac{b}{b+m\lambda} \right) \\ &= \frac{(b+\lambda)(b+2\lambda)}{b^2} \left(\frac{b}{\lambda} \right)^i \left(\left(\frac{b+\lambda}{\lambda} \right)_i \right)^{-1}, \quad i \geq 3, \end{aligned} \quad (96)$$

where the subscript $(x)_i = x(x+1)(x+2)\cdots(x+i-1)$ denotes ascending factorial (i.e. the Pochhammer symbol). Defining $\xi = b\lambda^{-1}$ then (C1) is satisfied provided

$$\lim_{i \rightarrow \infty} \frac{\xi^i}{(\xi+1)_i} = 0. \quad (97)$$

The function $\xi^i((\xi+1)_i)^{-1}$ is monotonically decreasing in both ξ and i and condition C1 is satisfied for any $\xi > 0$. Using $\xi = b\lambda^{-1}$ the expression (96) implies

$$\begin{aligned} \Delta^{(1)} &= 2 + \frac{(\lambda+\lambda\xi)(2\lambda+\lambda\xi)}{\lambda^2\xi^2} \sum_{i=3}^{\infty} i \frac{\xi^i}{(\xi+1)_i} \\ &= 2 + \frac{(\lambda+\lambda\xi)(2\lambda+\lambda\xi)}{\lambda^2\xi^2} \left(\frac{\xi^3}{2+3\xi+\xi^2} \right) = 2 + \xi. \end{aligned}$$

Thus we have

$$\Delta^{(1)} = 2 + \frac{b}{\lambda}, \quad (98)$$

and it follows that p_2^* , for $\nu = 1$, is determined by the formula

$$p_2^* = \frac{\lambda(k_0 - k_n m_0^2)}{2(k_+ m_0 + \lambda)(\lambda - k_2 \sigma_0)}. \quad (99)$$

References

- [1] John A Hardy and Gerald A Higgins. Alzheimer’s disease: the amyloid cascade hypothesis. *Science*, 256(5054):184–186, 1992.
- [2] John Hardy and David Allsop. Amyloid deposition as the central event in the aetiology of alzheimer’s disease. *Trends in pharmacological sciences*, 12:383–388, 1991.
- [3] Dennis J Selkoe and John Hardy. The amyloid hypothesis of Alzheimer’s disease at 25 years. *EMBO molecular medicine*, 8(6):595–608, 2016.
- [4] Andrew Bacyinski, Maosheng Xu, Wei Wang, and Jiani Hu. The paravascular pathway for brain waste clearance: Current understanding, significance and controversy. *Front. Neuroanat.*, 11:101, 2017.
- [5] H Benveniste, X Liu, S Koundal, S Sanggaard, H Lee, and J Wardlaw. The glymphatic system and waste clearance with brain aging: A review. *Gerontology*, 65:106–119, 2019.
- [6] Jenna Tarasoff-Conway, Roxana Carare, and Mony J. et. al. de Leon. Clearance systems in the brain—implications for Alzheimer disease. *Nat Rev Neurol*, 11(8):457–470, 2015.
- [7] Shu-Hui Xin, Lin Tan, Xipeng Cao, Jin-Tai Yu, and Lan Tan. Clearance of Amyloid Beta and Tau in Alzheimer’s Disease: from Mechanisms to Therapy. *Neurotoxicity Research*, 34(3):733–748, 2018.
- [8] G. Meisl, X. Yang, E. Hellstrand, B. Frohm, J. Kirkegaard, S. Cohen, C. Dobson, S. Linse, and T. Knowles. Differences in nucleation behavior underlie the contrasting aggregation kinetics of the aA β 40 and A β 42 peptides. *Proceedings of the National Academy of Sciences*, 111(26):9384–9389, 2014.
- [9] Samuel IA Cohen, Michele Vendruscolo, Mark E Welland, Christopher M Dobson, Eugene M Terentjev, and Tuomas PJ Knowles. Nucleated polymerization with secondary pathways. I. time evolution of the principal moments. *The Journal of chemical physics*, 135(6):08B615, 2011.
- [10] Samuel IA Cohen, Michele Vendruscolo, Christopher M Dobson, and Tuomas PJ Knowles. Nucleated polymerization with secondary pathways. II. determination of self-consistent solutions to growth processes described by non-linear master equations. *The Journal of chemical physics*, 135(6):08B611, 2011.
- [11] Samuel IA Cohen, Michele Vendruscolo, Christopher M Dobson, and Tuomas PJ Knowles. Nucleated polymerization with secondary pathways. III. equilibrium behavior and oligomer populations. *The Journal of chemical physics*, 135(6):08B612, 2011.
- [12] G. Meisl, J. Kirkegaard, P. Arosio, T. Michaels, M. Vendruscolo, C. Dobson, S. Linse, and T. Knowles. Molecular mechanisms of protein aggregation from global fitting of kinetic models. *Nature protocols*, 11(2):252, 2016.

- [13] Rebecca Frankel, Mattias Törnquist, Georg Meisl, Oskar Hansson, Ulf Andreasson, Henrik Zetterberg, Kaj Blennow, Birgitta Frohm, Tommy Cedervall, Tuomas PJ Knowles, et al. Autocatalytic amplification of Alzheimer-associated A β 42 peptide aggregation in human cerebrospinal fluid. *Communications biology*, 2(1):1–11, 2019.
- [14] Franziska Kundel, Liu Hong, Benjamin Falcon, William A McEwan, Thomas CT Michaels, Georg Meisl, Noemi Esteras, Andrey Y Abramov, Tuomas JP Knowles, Michel Goedert, et al. Measurement of tau filament fragmentation provides insights into prion-like spreading. *ACS chemical neuroscience*, 9(6):1276–1282, 2018.
- [15] Samuel IA Cohen, Sara Linse, Leila M Luheshi, Erik Hellstrand, Duncan A White, Luke Rajah, Daniel E Otzen, Michele Vendruscolo, Christopher M Dobson, and Tuomas PJ Knowles. Proliferation of amyloid- β 42 aggregates occurs through a secondary nucleation mechanism. *Proceedings of the National Academy of Sciences*, 110(24):9758–9763, 2013.
- [16] S. Linse, T. Scheidt, K. Bernfur, M. Vendruscolo, C. Dobson, S. Cohen, E. Sileikis, M. Lundquist, F. Qian, T. O’Malley, et al. Kinetic fingerprint of antibody therapies predicts outcomes of Alzheimer clinical trials. *bioRxiv*, page 815308, 2019.
- [17] D.L. Brody, H. Jiang, and N. et al. Wildburger. Non-canonical soluble amyloid-beta aggregates and plaque buffering: controversies and future directions for target discovery in Alzheimer’s disease. *Alz. Res. Therapy*, 9, 2017.
- [18] Formari S., Schäfer A., Goriely A., and Kuhl E. Spatially-extended nucleation-aggregation-fragmentation models for the dynamics of prion-like neurodegenerative protein-spreading in the brain and its connectome. *J. Theor. Biol.*, 2019.
- [19] M. Bertsch, B. Franchi, N. Marcello, M. C. Tesi, and A. Tosin. Alzheimer’s disease: a mathematical model for onset and progression. *Mathematical Medicine and Biology*, page dqw003, 2016.
- [20] S. Fornari, A. Schäfer, E. Kuhl, and A. Goriely. Spatially-extended nucleation-aggregation-fragmentation models for the dynamics of prion-like neurodegenerative protein-spreading in the brain and its connectome. *Journal of Theoretical Biology*, 486:110102, 2020.
- [21] J. Sotomayor. Generic bifurcations of dynamical systems. In *Dynamical systems*, pages 561–582. Elsevier, 1973.
- [22] J. Guckenheimer and P. Holmes. *Nonlinear oscillations, dynamical systems and bifurcations of vector fields*. Springer-Verlag, New York, 1983.
- [23] S. Wiggins. *Global bifurcations and chaos*. Springer-Verlag, New York Berlin, 1988.
- [24] A. Goriely. *Integrability and Nonintegrability of Dynamical Systems*. World Scientific Publishing Company, 2001.
- [25] A. Goriely. Painlevé analysis and normal forms theory. *Phys. D*, 152:124–144, 2001.
- [26] A. Newell. Envelope equations. *Lect. Appl. Math.*, 15, 1974.

- [27] G. Meisl. Modelling protein aggregation in-vitro and in-vivo. *Doctoral Dissertation*. University of Cambridge, 2016.